




OPEN

Understanding structure–properties relationships of porphyrin linked to graphene oxide through π – π -stacking or covalent amide bonds

Anna Lewandowska-Andralojc^{1,2}, Ewelina Gacka^{1,2}, Tomasz Pedzinski^{1,2}, Gotard Burdzinski³, Aleksandra Lindner⁴, Jessica M. O'Brien⁵, Mathias O. Senge^{5,6}, Aleksandra Siklitskaya⁷, Adam Kubas⁷, Bronislaw Marciniak^{1,2} & Justyna Walkowiak-Kulikowska¹

Two graphene oxide nanoassemblies using 5-(4-(aminophenyl)-10,15,20-triphenylporphyrin (TPPNH₂) were fabricated by two synthetic methods: covalent (GO-CONHTPP) and noncovalent bonding. GO-CONHTPP was achieved through amide formation at the periphery of GO sheets and the hybrid material was fully characterized by FTIR, XPS, Raman spectroscopy, and SEM. Spectroscopic measurements together with theoretical calculations demonstrated that assembling TPPNH₂ on the GO surface in DMF-H₂O (1:2, v/v) via non-covalent interactions causes changes in the absorption spectra of porphyrin, as well as efficient quenching of its emission. Interestingly, covalent binding to GO does not affect notably neither the porphyrin absorption nor its fluorescence. Theoretical calculations indicate that close proximity and π – π -stacking of the porphyrin molecule with the GO sheet is possible only for the non-covalent functionalization. Femtosecond pump–probe experiments revealed that only the non-covalent assembly of TPPNH₂ and GO enhances the efficiency of the photoinduced electron transfer from porphyrin to GO. In contrast to the non-covalent hybrid, the covalent GO-CONHTPP material can generate singlet oxygen with quantum yields efficiency ($\Phi\Delta = 0.20$) comparable to that of free TPPNH₂ ($\Phi\Delta = 0.26$), indicating the possible use of covalent hybrid materials in photodynamic/photothermal therapy. The spectroscopic studies combined with detailed quantum-chemical analysis provide invaluable information that can guide the fabrication of hybrid materials with desired properties for specific applications.

Among graphene derivatives, graphene oxide (GO) is particularly interesting due to functional groups capable of anchoring functional molecules through non-covalent/covalent interactions. One strategy to fabricate hybrid materials is to functionalize graphene with photochemically active molecules. Among dyes, porphyrins are well suited to construct graphene-based composites due to their excellent photoactive properties¹. Photoinduced electron transfer (PET) ability has prompted porphyrins to be widely used as photosensitizers in artificial photosynthetic devices^{1–5}. In addition, porphyrins are known for long-lived triplet states that enhance the formation of singlet oxygen through energy transfer, and this feature is also critical to improve the efficiency of photodynamic treatments^{6–8}.

¹Faculty of Chemistry, Adam Mickiewicz University, Uniwersytetu Poznańskiego 8, 61-614 Poznań, Poland. ²Center for Advanced Technology, Adam Mickiewicz University, Uniwersytetu Poznańskiego 10, 61-614 Poznań, Poland. ³Faculty of Physics, Adam Mickiewicz University, Uniwersytetu Poznańskiego 2, 61-614 Poznań, Poland. ⁴Helmholtz-Zentrum Dresden-Rossendorf, Institute of Ion Beam Physics and Materials Research, Bautzner Landstraße 400, 01328 Dresden, Germany. ⁵School of Chemistry, Chair of Organic Chemistry, Trinity Biomedical Sciences Institute, Trinity College Dublin, The University of Dublin, 152-160 Pearse Street, Dublin 2, Ireland. ⁶Institute for Advanced Study (TUM-IAS), Focus Group-Molecular and Interfacial Engineering of Organic Nanosystems, Technical University of Munich, 85748 Garching, Germany. ⁷Institute of Physical Chemistry, Polish Academy of Sciences, Kasprzaka 44/52, 01-224 Warsaw, Poland. ✉email: alewand@amu.edu.pl

Considering the above, it is timely and important to prepare hybrid materials consisting of graphene and photoactive units such as porphyrins and study their behavior in the context of application in solar energy conversion or photodynamic therapy. The conversion of light energy to energy-rich molecules (solar fuel) through photocatalytic processes starts with the photoinduced generation of energy-rich electrons. Therefore, the PET process in those hybrid materials plays a key role in converting solar light into chemical energy or electricity. The occurrence of PET in hybrid materials consisting of porphyrins and graphene materials has been demonstrated for several systems^{9–12}, and efficient PET has also been shown to enhance photocatalytic hydrogen production^{13,14}.

In addition to solar energy conversion, an association of different graphene oxides with photosensitizers has allowed the development of multifunctional photodynamic/photothermal platforms for tumor ablation and metastasis prevention^{15–18}. The use of graphene oxides in PDT (photodynamic therapy) is more challenging since the electron acceptor capability of graphene counteracts the generation of ROS (reactive oxygen species). Disabling this alternative deactivation channel is mandatory to assure good ROS production.

Elucidating the factors that affect the efficiency of PET and singlet oxygen generation in porphyrin/graphene materials is crucial for knowledge-driven the design of nanomaterials and their use in solar-energy conversion or PDT.

One of the most critical factors influencing the interaction between porphyrin and graphene material is the synthesis protocol for the composites. Generally, the synthesis of dye/graphene oxide composites requires either covalent or non-covalent functionalization^{19–21}. The non-covalent strategy relies on fundamental molecular interactions such as π - π -stacking, hydrogen bonding, or charge attraction between graphene and organic molecules. Covalent functionalization reactions such as the formation of amide or ester linkages are more complex; however, the resulting composite materials are more stable.

Surprisingly, despite these recent advances in the field of porphyrin/graphene nanoassemblies, there are no reports comparing covalent and non-covalent functionalization of graphene oxide with the same porphyrin. Therefore, in the present contribution, we fabricated two GO nanoassemblies using 5-(4-(aminophenyl)-10,15,20-triphenylporphyrin (TPPNH₂) using two different synthetic methods: covalent (GO-CONHTPP) and non-covalent (GO-TPPNH₂) bonding. The main objective of the current study was to elucidate whether the type of functionalization covalent vs. non-covalent is privileged for photoinduced electron transfer or singlet oxygen generation. Time-resolved spectroscopic measurements revealed that only the non-covalent assembly of TPPNH₂ and GO enhances the efficiency of the photoinduced electron transfer from the porphyrin to GO. In contrast to the non-covalent hybrid, the covalent GO-CONHTPP material can generate singlet oxygen with comparable yields to free TPPNH₂, indicating the possible use of covalent hybrid materials in photodynamic/photothermal therapy. The results clearly demonstrate that the type of functionalization: covalent vs. non-covalent affects the hybrid properties and thus their potential application.

Experimental

Reagents and materials. Graphene oxide (GO-powder <35 mesh. C/O atomic ratio = 2.5–2.6) was purchased from LayerOne. Anhydrous DMF and tris(2,2'-bipyridyl)ruthenium(II) chloride hexahydrate were purchased from Sigma Aldrich. Reagents for porphyrin synthesis were obtained from commercial sources and were used as received. For solution preparation ultrapure water (18 M Ω cm) was used. The synthesis of TPPNH₂ followed a literature procedure²² and is described in the Supporting Information along with ¹H NMR and MALDI spectra (Figs. S1–S3). For all experiments GO or GO-CONHTPP hybrid suspensions were prepared by dispersing GO or hybrid powder in DMF or DMF-H₂O (1:2, v/v) followed by ultrasonication for 30 min.

Experimental apparatus. UV-Vis absorption spectra were recorded using a two-beam spectrometer Cary 100 UV-Vis scanning from 200 to 800 nm with 1 nm increments. Fluorescence spectra were recorded in the range of 500 and 800 nm on a LS 50B spectrofluorometer (Perkin Elmer) for solutions with an absorbance at the excitation wavelength lower than 0.1. Quantitative analysis of fluorescence data of graphene-containing materials is complicated by light absorption and scattering by the GO; therefore, to obtain meaningful emission data, the absorbance of free TPPNH₂ and TPPNH₂ attached to GO was adjusted to be identical at the excitation wavelength (0.05); in addition, the inner filter correction for the GO absorption of the excitation light was applied²³. The fluorescence lifetimes were measured on a Fluorescence Lifetime Spectrometer (FluoTime300 from PicoQuant) with a detection system based on time-correlated single-photon counting (TCSPC). The emission decay lifetimes were measured following excitation with 408 nm diode laser. In addition, for the analysis of a fluorescence decay, an instrument response function (IRF) was obtained using Ludox solution (colloidal silica). The direct measurements of singlet oxygen emission were carried out on a FluoTime 300 fluorescence spectrophotometer with an NIR PMT detector H10330-45 (Hamamatsu) equipped with an 1000 nm long-pass filter. The samples were excited at 408 nm or 440 nm using a high repetition rate 40 MHz picosecond laser diode (LDH-405 and LDH-440, PicoQuant). Data collection was performed using a computer-mounted PCI-board multichannel scaler (NanoHarp 250, PicoQuant). The porphyrin absorbance was maintained at about 0.1 at the excitation wavelength. The time-resolved measurements (decay traces at $\lambda = 1270$ nm) were collected using a so-called “burst mode”, in which the sample was first excited using multiple pulses of the laser (1000 pulses every 25 ns giving a 25 μ s excitation “burst”) to build up the population of singlet oxygen and then left to decay in the 100 μ s time window of the experiment. Samples were placed in 10 mm \times 10 mm quartz cells for all steady-state and time-resolved emission measurements. The quantum yields could also be determined from the recorded phosphorescence spectra; however, the time-resolved method seems to be more reliable due to the spectral overlap of different emissions at 1270 nm (e.g., for TPPNH₂ most likely due to the 2nd order diffraction of the emission band and the characteristics of the cut-off filters used). The use of the “quasi time-gated” method discriminates the much faster emission from the relatively slow decay of the singlet oxygen phosphorescence.

Details of the femtosecond transient absorption spectroscopy setup have been described elsewhere²⁴. In short, the ultrafast laser system consisted of a short-pulse titanium sapphire oscillator (Mai Tai, Spectra Physics, 70 fs) followed by a high-energy titanium sapphire regenerative amplifier (Spitfire Ace, Spectra Physics, 100 fs). The 800 nm beam was split into two beams to generate: (1) a pump ($\lambda_{\text{exc}} = 420$ nm and 440 nm) from the optical parametric amplifier (Topas Prime with a NirVis frequency mixer) and (2) probe pulses in the UV–Vis range by using sapphire plate (Ultrafast Systems, Helios). The temporal resolution of the setup is about 300 fs. For transient UV–Vis measurements a quartz cell with 2 mm optical path of solution was used with the absorbance of about 0.2 at the excitation wavelength. The sample solution was stirred by a Teflon-coated bar. Typical pump energy was about 2 μJ . All experiments were performed at room temperature. Analysis of the transient absorption data was made using Surface Explorer software (Ultrafast Systems). The Fourier Transform Infrared Spectra (FTIR) were recorded with Bruker FT-IR IFS 66/s spectrometer (sample as tablet with KBr). NMR spectroscopy was carried out on a Bruker DPX 400 (400 MHz for ^1H NMR) spectrometer at room temperature using an appropriate deuterated solvent. Mass spectrometry results (HRMS) were obtained using a Q-ToF Premier Waters MALDI quadrupole time-of-flight (Q-TOF) mass spectrometer equipped with a Z-spray electrospray ionization (ESI) and a matrix assisted laser desorption ionization (MALDI) sources in positive mode with *trans*-2-[3-(4-*tert*-butylphenyl)-2-methyl-2-propenylidene]malononitrile as the internal matrix. A Digital Stuart SMP10 melting point apparatus was used to determine all melting points, which are uncorrected. Samples for imaging were prepared by drop-casting solution/suspension of interest onto silicon wafer and drying in air. The morphology of samples was examined by scanning electron microscopy (SEM) Quanta 250 FEG, FEI. The measurements were performed in high vacuum using accelerating voltage 2 kV. X-ray photoelectron spectroscopy (XPS) measurements were performed using a SPECS-XPS photoelectron spectrometer. Samples for XPS measurements were prepared by dropping the dilute colloidal dispersion onto a silicon wafer and dried in the air at room temperature. Raman spectra of the samples were recorded on a LabRamHR Evolution spectrometer from Horiba Scientific coupled to a BFXM microscope (Olympus) with $\times 100_{\text{Vis_LWD}}$ objective, using a Nd:YAG laser with a wavelength of 532 nm. Samples for Raman measurements were prepared by drop-casting a solution of TPPNH₂ and a suspension of GO and GO-CONHTPP onto silicon wafers and drying in air.

Computational details. We followed closely the protocol validated in our previous studies^{25–27}. Briefly, the GO was represented as C₅₉O₂₆H₂₆ Lerf-Klinowski-type model that was shown to be robust in analyzing non-covalent functionalization with porphyrins²⁷. The structures of free TPPNH₂ and two hybrids (covalent GO-CONHTPP and noncovalently interacting GO/TPPNH₂) were optimized at the density functional theory (DFT) level using BP86 functional²⁸ augmented with D3BJ^{29,30} and gCP³¹ corrections to improve the description of dispersion interactions and to compensate for the basis set superposition error, respectively. This setup is abbreviated as BP86 + D3gCP. The structures obtained were subjected to numerical second derivative calculations to confirm their character as true energy minima at the potential energy surface. Single-point calculations at optimized structures were performed using B3LYP functional³² to decrease electron delocalization error and provide data directly comparable to our previous studies. The basis set applied was def2-TZVP³³. All DFT calculations were performed using ORCA 4.2.0 program³⁴. The numerical overlap between selected orbitals was calculated with Multiwfn 3.6³⁵.

Results and discussion

Synthesis and characterization. The covalent linkage of GO and TPPNH₂ was obtained by direct coupling of the GO carboxylic groups with the amino group of TPPNH₂ to form an amide in one-step^{36–40}, as illustrated in Fig. 1. For comparison, GO non-covalently functionalized with TPPNH₂ was prepared by simple mixing and sonication of GO and TPPNH₂ dispersions.

GO-CONHTPP nanohybrid was characterized via FTIR, Raman and XPS spectroscopy and scanning electron microscopy (SEM) (Fig. 2 and Figs. S4–S6) which provided evidences for successful functionalization of GO with TPPNH₂. In the FTIR spectrum of the covalent nanohybrid signals characteristic for porphyrin are noticed (red stars in Fig. S4), among others at 800 cm⁻¹ and 734 cm⁻¹, which were not present in the spectrum of GO itself. At the same time, bands characteristic for the N–H stretching vibrations in the NH₂ amino groups are absent. Additionally, the signal at 1734 cm⁻¹ characteristic of the carbonyl in carboxylic groups disappears, and a new band at 1650 cm⁻¹ appears, which can be attributed to amide C=O stretching. Likewise, a new band at 1450 cm⁻¹, not observed for free TPPNH₂ and GO, can be attributed to the stretching vibrations of the C–N bonds in amide groups. These results indicate that the TPPNH₂ molecules are covalently bound to the graphene oxide via amide linkages.

In the Raman spectra for the covalent nanocomposite, Raman peaks characteristic of the porphyrin macrocycle are visible in the spectra (Fig. S5). No shifts of the porphyrin signals after TPPNH₂ attachment to the GO sheets were observed, which indicates lack of the close contact (π – π stacking) between the surface of the GO sheets and the porphyrin macrocycles, in accordance with further presented data.

X-ray photoelectron spectroscopy (XPS, Fig. 2) shed more light on the structure of starting material GO and the functionalized material GO-CONHTPP. The oxygen content in GO is ca. 30.7 atom %, which suggests a high degree of oxidation of the starting material. The XPS spectra of C1s for GO were deconvoluted into four peaks, 283.5, 284.6, 286.5, 288.4 eV, corresponding to the characteristic peaks of C–C, C=C, C–O, O–C=O, respectively (Fig. 2A). Compared with GO, the oxygen-containing functional group (O–C=O, C=O, C–O–C, and C–OH) peaks of GO-CONHTPP decrease sharply, while the sp² C=C bond carbon peak (284.5 eV) increases significantly. The total C/O atomic ratio for GO-CONHTPP increased to 7.7 from 2.1 of GO, clearly demonstrating a reduction of GO during the functionalization process.

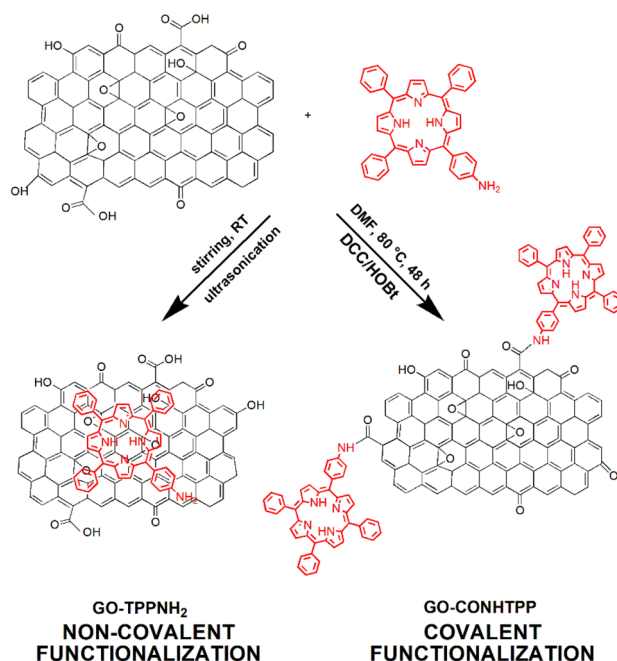


Figure 1. Schematic illustration for the preparation of GO with covalently and non-covalently linked TPPNH₂; DCC—*N,N'*-dicyclohexylcarbodiimide, HOBt—1-hydroxybenzotriazole.

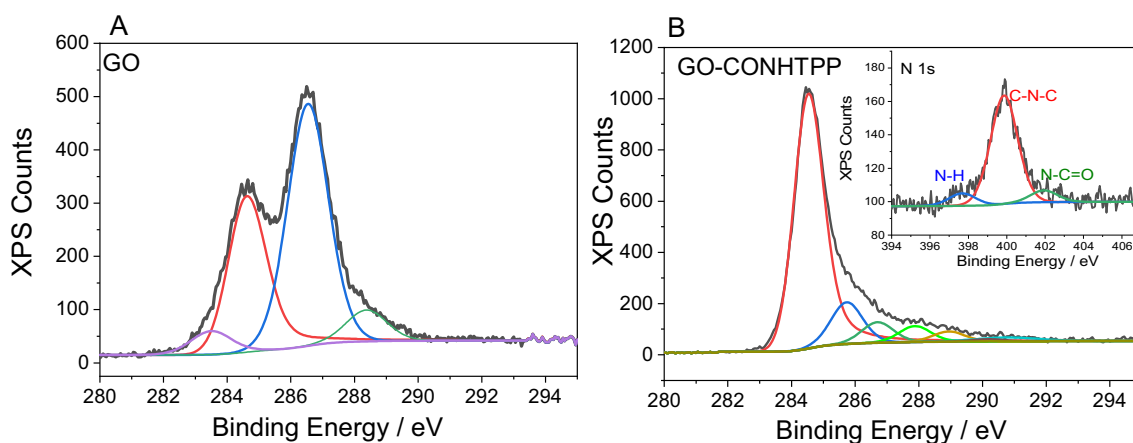


Figure 2. XPS spectra of C1s for (A) GO and (B) GO-CONHTPP and N1s for GO-CONHTPP in the inset.

The binding of TPPNH₂ molecules to GO was further confirmed by the increased content of nitrogen by 0.3% in comparison to the GO material subjected to the same synthetic procedure in the absence of porphyrin. This relates to a calculated porphyrin content in the hybrid material of 2.7% by weight. Due to the limited number of carboxylic groups on GO, the functionalization degree is low and comparable to other porphyrins attached to GO via an amide bond⁴¹.

A typical N1s XPS for free base porphyrins shows two components arising from the macrocycle's two inequivalent nitrogen atoms, which are usually separated by approximately 2 eV^{42,43}. The N1s spectra were deconvoluted into three peaks (inset in Fig. 2B). The peak at 397.7 eV originates from the iminic nitrogen, while the one at 399.9 eV is attributed to the pyrrolic nitrogen. The third peak at 401.9 eV is assigned to N–C=O. The presence of the latter peak indicated that TPPNH₂ was linked to the GO via amide bonds.

Photophysical characterization. *Absorption properties.* The absorption spectra of TPPNH₂ in DMF and DMF–H₂O (1:2, v/v) exhibited the expected porphyrin-specific bands, i.e. the Soret and four Q-bands (Fig. S7). In DMF–H₂O (1:2, v/v) the Soret band of TPPNH₂ is red-shifted by 2 nm compared to DMF, and the band is slightly broadened. The presence of the characteristic Soret and Q bands in UV–Vis spectrum of GO-CONHTPP validates the existence of porphyrin in the nanocomposites (Fig. 3).

Interestingly, no shift of the TPPNH₂ Soret band at 419 nm is observed upon covalent binding to the GO sheets, which is in agreement with the report by Xu et al.⁴⁴. The only difference in the UV–Vis spectra of TPPNH₂

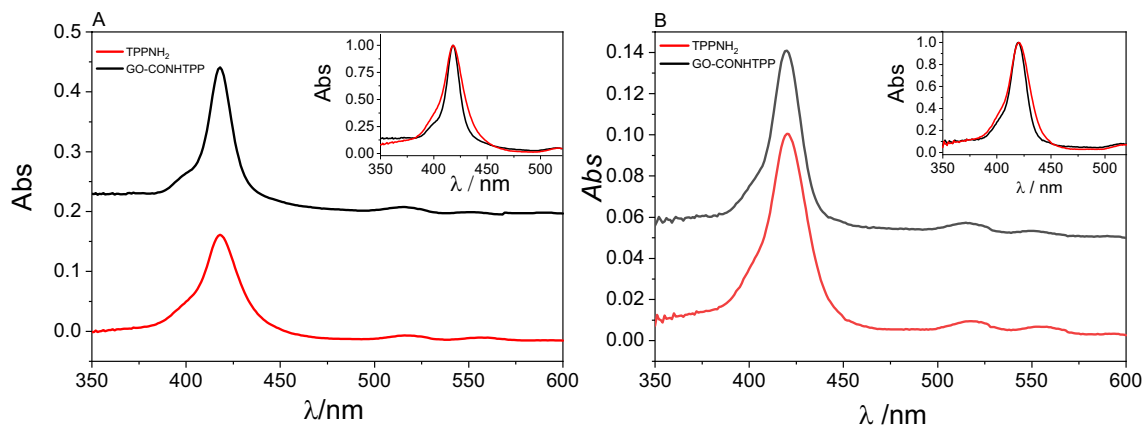


Figure 3. Absorption spectra of free TPPNH₂ (red curve), TPPNH₂ covalently bound to GO (black curve) in: (A) DMF, (B) DMF-H₂O (1:2 v/v). Insets: Normalized absorption spectra of TPPNH₂ and GO-CONHTPP.

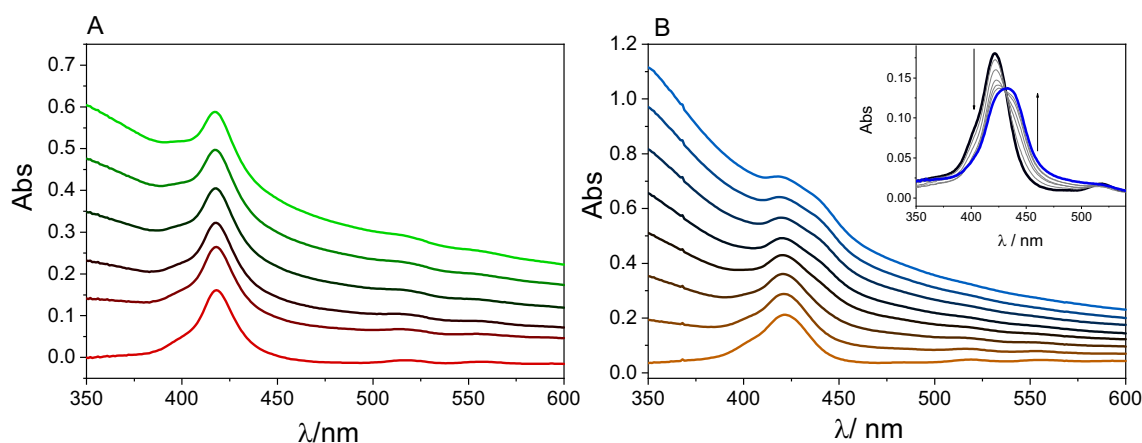


Figure 4. Absorption spectra recorded for 3 mL of 0.7 μM solution of TPPNH₂ in: (A) DMF with GO dispersion (0–0.066 mg mL⁻¹), (B) DMF-H₂O (1:2, v/v) with GO dispersion (0–0.1 mg mL⁻¹). The inset highlights the Soret band region with the spectra corrected for GO absorption.

attached to the GO versus free TPPNH₂ is a slight broadening of the Soret band of the latter. The broadening of the TPPNH₂ Soret band may indicate aggregation of the porphyrin molecules, which is presumably inhibited once TPPNH₂ is bound to GO.

The absorption spectra of GO-CONHTPP in DMF-H₂O (1:2 v/v) also largely resemble the UV-Vis spectra of the free porphyrin (Fig. 3B). The lack of noticeable changes in TPPNH₂ absorption upon covalent functionalization to GO might be explained by the rigid amide bond preventing TPPNH₂ molecules from interacting via π - π stacking with the GO surface they are linked to. Other related covalent systems, which were formed via amide or ester linkage between -COOH at the edges of GO surface and porphyrin, also exhibited lack of significant change in the Soret band position^{41,45}. However, the position of the Soret band was found to be red-shifted for covalent hybrids when porphyrin was used with a modified longer amide axial ligand or when porphyrin was attached directly to the GO surface using an epoxy group present on the surface^{46,47}. These examples indicate that π - π stacking between hybrid components is essential to observe changes in the UV-vis spectra of the porphyrin. In our study the lack of π - π stacking between TPPNH₂ molecules and the GO surface has been further confirmed by calculating theoretically the structure of the hybrid material (vide infra).

To compare the interactions between TPPNH₂ bound covalently or non-covalently to the GO, the optical absorption spectra of a series of TPPNH₂ solutions in which GO was gradually added to a TPPNH₂ solution were measured (Fig. 4). No significant spectroscopic changes occur when titrating the TPPNH₂ solution with GO suspension in DMF (Fig. 4A). After centrifuging the mixture of TPPNH₂ and GO in DMF, virtually all TPPNH₂ was still present in the supernatant, and GO was collected as the precipitate. This indicates that the interaction between TPPNH₂ and GO in DMF is weak.

Conversely, changes in the UV-Vis spectra were noted when titrating in DMF-H₂O (1:2, v/v) (Fig. 4B). The intensity of the original Soret band at 421 nm gradually decreased, and a new Soret band appeared at 440 nm, together with the presence of isosbestic point at 430 nm (inset in Fig. 4B). The Soret band was found to be red-shifted by 19 nm for TPPNH₂ adsorbed on the GO surface and slightly broadened in comparison to free TPPNH₂ (Fig. S8).

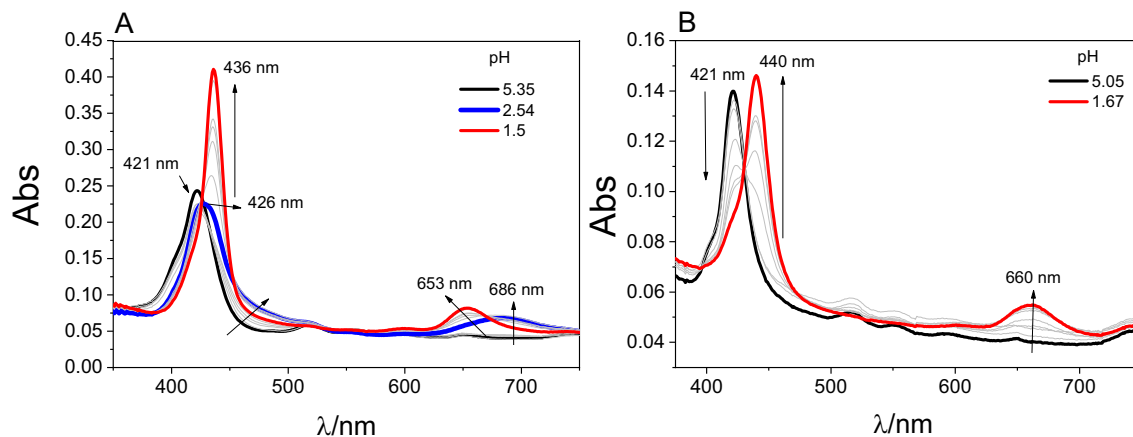


Figure 5. Absorption spectra recorded during the addition of 1 M HCl to a solution of: (A) TPPNH₂ and (B) GO-CONHTPP in DMF-H₂O (1:2, v/v).

The bathochromic shift observed upon nanohybrid formation could be attributed to a decrease in the meso-phenyl substituents tilt angle adsorbed on the GO sheet as described previously for related hybrids porphyrin-GO^{25–27}. Interestingly, three of the four Q bands disappeared for TPPNH₂ adsorbed on the GO surface in DMF-H₂O (1:2, v/v), and a new broad band was observed at 659 nm (Fig. S8). The presence of an intense long-wavelength band can be explained by partial charge transfer from TPPNH₂ to the GO sheet what is supported by our theoretical calculations (vide infra) and similarity with literature data on porphyrin radical cation spectra^{12,48,49}.

Centrifugation of the mixture of TPPNH₂ and GO allows efficient nanohybrid isolation (Fig. S9). Based on the minor peak attributed to porphyrin in the UV-Vis spectrum of the supernatant, it is clear that all of the nanohybrids obtained were successfully collected as a precipitate. This experiment confirms that GO can be successfully functionalized non-covalently with TPPNH₂ in DMF-H₂O (1:2, v/v) by simply mixing solutions of the two components. Based on this experiment, it was estimated that the maximum amount of TPPNH₂ that can be adsorbed on the GO surface is 1.3%. This is similar to values reported for other non-covalent hybrids of GO with neutral porphyrins, such as 5,10,15,20-tetra(hydroxyphenyl)porphyrin or its zinc derivative^{13,25,26}.

In summary, the presence of water favors the formation of stable non-covalent GO-TPPNH₂ hybrids. While the absorption spectrum of porphyrin remains unchanged for GO-CONHTPP compared to free porphyrin, for TPPNH₂ adsorbed non-covalently to GO, the absorption spectra differ significantly in DMF-H₂O (1:2, v/v). Our results demonstrate that the type of GO functionalization—covalent vs. non-covalent—affects the ground state electronic structure of the porphyrin.

The structure of covalent and non-covalent hybrid materials predicted by theoretical calculations revealed that close proximity and π - π stacking interaction of the porphyrin molecule with the GO sheet is only possible for the non-covalent functionalization. Based on the results described above, it can therefore be concluded that π - π stacking interaction is required to modify the electronic structure of the porphyrin which is manifested by the changes in the electronic absorption spectra. This is consistent with previous reports demonstrating that red-shift of the Soret band for covalent hybrids is observed only when porphyrin with a modified longer amide axial ligand was used or when the porphyrin was attached directly to the GO surface using an epoxy group present on the surface^{46,47}.

Spectroscopic measurements as a function of pH were used to provide additional evidence for the covalent attachment of TPPNH₂ to GO. Changes in TPPNH₂ towards acidic pH introduce positive charge to neutral TPPNH₂ in two steps corresponding to protonation of peripheral amine -NH₂ and the imine nitrogens in the core (Fig. S10). Spectra of acid-titration of TPPNH₂ clearly demonstrates two well-separated stages (pK_a 3.01 and 2.01) both indicated by isosbestic points (Fig. 5 and Fig. S11).

Titration of hybrid GO-CONHTPP with acid gave only a single isosbestic point with the pK_a of 2.36; hence, only core protonation occurred (Fig. 5B and Fig. S12). This experiment proves that there is no free amine group in TPPNH₂ when it is attached to the GO and no free porphyrin remains in the hybrid after synthesis.

Emission properties. To investigate the excited state interactions of TPPNH₂ and graphene oxide in the hybrid, the fluorescence spectra of the TPPNH₂ and GO-CONHTPP hybrid were compared. Surprisingly, compared to TPPNH₂, GO-CONHTPP demonstrates even higher fluorescence intensity after applying the appropriate inner filter correction (the intensity was lower for uncorrected spectra). This is contrary to previously reported data for TPPNH₂ covalently functionalized with graphene^{41,44}. This difference may arise either from difficulties in the quantitative analysis of emission data for graphene-based materials or from different electronic interactions between the components of the hybrid materials. The interactions between TPPNH₂ and GO depend on the exact structure of GO, which strongly depends on the synthesis protocol^{41,44}. In both studied solvents for GO-CONHTPP, the emission at 665 nm is blue-shifted by ca. 10 nm compared to free TPPNH₂, consistent with previous findings (Fig. 6A)^{41,44}. Porphyrins are known to aggregate strongly^{50–54}, and therefore, the decrease in fluorescence intensity in comparison with GO-CONHTPP and the shift in the emission of free TPPNH₂

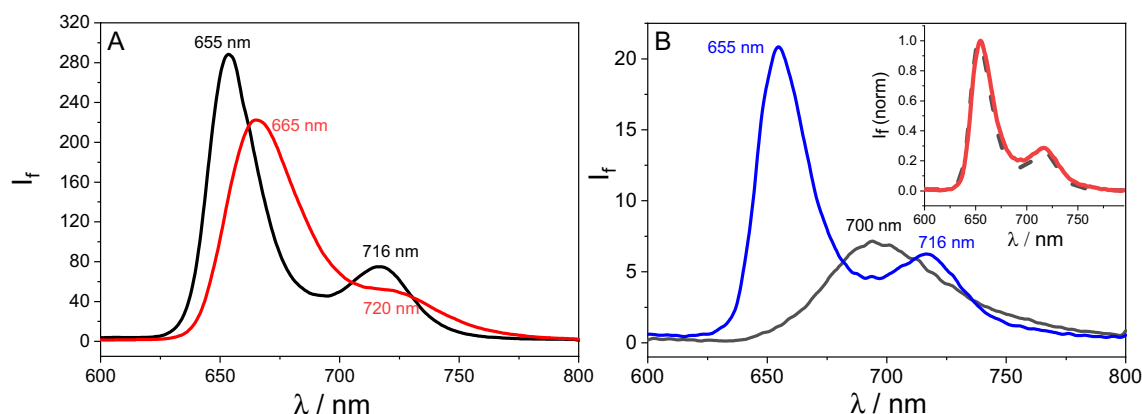


Figure 6. (A) Emission properties of TPPNH₂ (red) and GO-CONHTPP (black) in DMF, $\lambda_{\text{exc}} = 419$ nm. (B) Fluorescence spectra registered for TPPNH₂ after the addition of 20 μL of 1 M HCl at two excitation wavelengths: 419 nm (blue) and 450 nm (black). Inset: Normalized fluorescence spectra of GO-CONHTPP in DMF and TPPNH₂ at excitation wavelength 419 nm in acidified DMF.

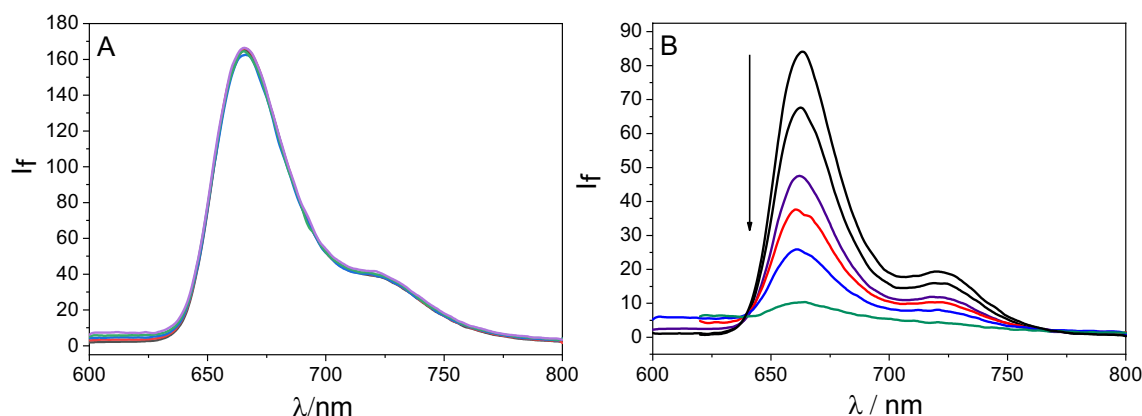


Figure 7. The emission spectra of TPPNH₂ recorded during addition of a suspension of GO (0–0.067 mg mL⁻¹). In: (A) DMF, $\lambda_{\text{exc}} = 419$ nm, (B) DMF-H₂O (1:2, v/v), $\lambda_{\text{exc}} = 430$ nm. Spectra were corrected for the inner filter effects I and II.

can be explained by aggregation. As presented in Fig. S13, the fluorescence excitation spectrum recorded for GO-CONHTPP and TPPNH₂ solution corresponds to their absorption spectrum, although the latter is slightly broadened. To verify the hypothesis of free TPPNH₂ aggregation, we measured the emission spectra of free TPPNH₂ in DMF after addition of 20 μL of 1 M HCl which results in an equilibrium state between neutral and protonated porphyrin (Fig. 6B). Excitation at 450 nm leads to recording the emission spectra of protonated TPPNH₂, which is broad with the maximum at 700 nm⁵⁵. Upon excitation at 419 nm, emission from neutral TPPNH₂ present in acidic DMS was observed with maximum at 655 nm which matches the emission spectrum of the nanocomposites GO-CONHTPP (see inset in Fig. 6B). The addition of a small amount of HCl to TPPNH₂ solution in DMF destroys the aggregates due to the repulsive interaction of the protonated molecules. The molecules become non-planar and hence cannot aggregate⁵⁶. Therefore, the emission spectra of neutral TPPNH₂ molecules in acidic DMF coincide with those recorded for the covalent GO-CONHTPP composites in both DMF and DMF-H₂O (1:2, v/v).

For comparison, the interaction of the singlet excited state of TPPNH₂ non-covalently attached to GO sheets was investigated by emission spectroscopy. Upon correcting the experimental data for absorption of the excitation light by GO and the absorption of TPPNH₂ emission by GO, it was found that in DMF no fluorescence quenching occurred at all (Fig. 7A). In contrast a significant decrease in the TPPNH₂ fluorescence intensity was observed with increasing GO concentration in DMF-H₂O (1:2, v/v) but with no observable changes in the peak shape and position (Fig. 7B). Moreover the fluorescence excitation spectrum of TPPNH₂ after the addition of GO, corresponded to the absorption spectrum of unbound TPPNH₂ (Fig. S15). This indicates that the non-covalent nanohybrid TPPNH₂-GO is not emissive or only a very weakly emissive material in DMF-water mixture. A possible reason for the non-emissivity of TPPNH₂-GO complex is the existence of a competitive very fast non-radiative process that deactivates singlet excited state.

In summary, firstly, steady-state absorption and emission measurements show that the interaction strength between TPPNH₂ and GO can be modulated by the choice of solvent system. Secondly, data from fluorescence

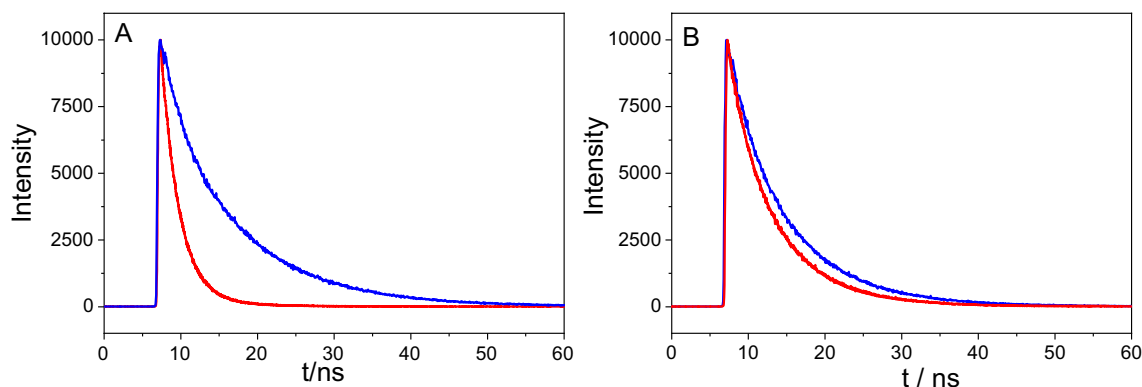


Figure 8. Decay of a fluorescence recorded for TPPNH₂ (red) and GO-CONHTPP (blue) in: (A) DMF and (B) DMF-H₂O (1:2, v/v) ($\lambda_{\text{ex}} = 405 \text{ nm}$, $\lambda_{\text{em}} = 650 \text{ nm}$).

spectra indicate that there is no interaction of the singlet excited state of the porphyrin with GO in covalent composites in both solvent systems studied, similarly like for the in non-covalent composites in DMF.

To further probe the possible interaction of the singlet excited state of porphyrin functionalized covalently and non-covalently with GO we used time-correlated single photon counting. The fluorescence lifetime of TPPNH₂ in DMF extracted from the fluorescence decay was approximately 2.4 ns and 8.6 ns for free TPPNH₂ and GO-CONHTPP, respectively (Fig. 8A). The corresponding values in DMF-H₂O (1:2, v/v) were 5.2 ns and 8.1 ns for free TPPNH₂ and GO-CONHTPP, respectively (Fig. 8B). The longer fluorescence lifetime for GO-CONHTPP is in agreement with the higher emission intensity measured in steady-state experiment. A possible reason is that unbound TPPNH₂ molecules in solution are prone to form aggregates, whereas covalent attachment to GO prevents formation of aggregates, at least at low concentration. It is well known that porphyrin aggregates are characterized by lower emission intensity or even lack of fluorescence in comparison to monomers⁵⁷. To clarify this point further, we performed time-resolved emission measurements with different TPPNH₂ concentrations which revealed a strong dependence of the TPPNH₂ fluorescence lifetime on its concentration (Fig. S16). Therefore, the formation of TPPNH₂ aggregates hinders direct comparison of the emission properties of the free monomer of TPPNH₂ and covalently attached to GO.

The possible interaction of the TPPNH₂ singlet excited state with GO was further examined by monitoring the emission decay profiles of TPPNH₂ in the presence of different GO concentrations. When GO was added to TPPNH₂, the lifetime remained practically unaltered and insensitive to its concentration (Fig. S17). Lack of observable change in the singlet excited state lifetime of free TPPNH₂ excludes dynamic quenching by GO. Taking into account results from both steady-state and time-resolved emission experiments, it can be stated that the observed emission quenching of TPPNH₂ upon addition of GO is due to static quenching.

Femtosecond transient absorption spectroscopy. Of particular interest was the investigation of a possible electron transfer process from the singlet excited state of the porphyrin to graphene oxide sheets, as this process is crucial for potential applications in solar energy conversion. The singlet excited state differential absorption measured immediately after the 422 nm laser pulse excitation of unbound TPPNH₂ showed strong absorption around 450–500 nm and a Q-band bleaching, consistent with the Q band position observed in the UV-Vis absorption spectra (Fig. 9A).

Kinetic profile analysis revealed the presence of two exponential decays of the transient absorption signal at 452 nm with time constants of 14 and 206 ps (Fig. S18). The residual absorption observed as a small offset which does not vanish over the entire experimental time window (3 ns) (on Fig. S18 depicted for 452 nm and 520 nm) can be attributed to the triplet excited state. The decay profiles from fs transient absorption spectroscopy do not match the data obtained by the TCSPC technique. However, the femtosecond experiments were performed at 10 times higher porphyrin concentrations than in the TCSPC experiment. As discussed above, the fluorescence decay obtained by TCSPC method strongly varies with the porphyrin concentration. Therefore, the observed fast decays on the fs transient absorption spectroscopy could be attributed to the aggregates present in the sample.

The transient absorption and kinetic profiles of GO-CONHTPP covalent composites showed spectral features very similar to those registered for the free dye (see Fig. 9B) what indicates that electron transfer in the covalent hybrid material is very unlikely.

An analogous transient absorption (TA) experiment was performed when GO was added to a TPPNH₂ solution in DMF-H₂O (1:2, v/v) (Fig. 10A). The spectra presented in Fig. 10A were corrected for the transient absorbance of GO (Fig. S19)⁵⁸. Clearly, the TA spectra of TPPNH₂ non-covalently functionalized with GO (Fig. 10A) recorded just after excitation do not resemble the TA spectra obtained for free TPPNH₂ (Fig. 9A).

As presented in Fig. 10A, the formation of a broad band in the region of 450–650 nm was detected. This broad positive band can be attributed to the porphyrin radical cation based on the similarity to reported spectra for the related systems^{49,59}. The presence of the TPPNH₂ radical cation just after the laser pulse in the system, where TPPNH₂ was simply mixed with GO, provides evidence for fast photoinduced electron transfer from the porphyrin to GO. The absorption profile at 550 nm attributed to the TPPNH₂ radical cation disappears with

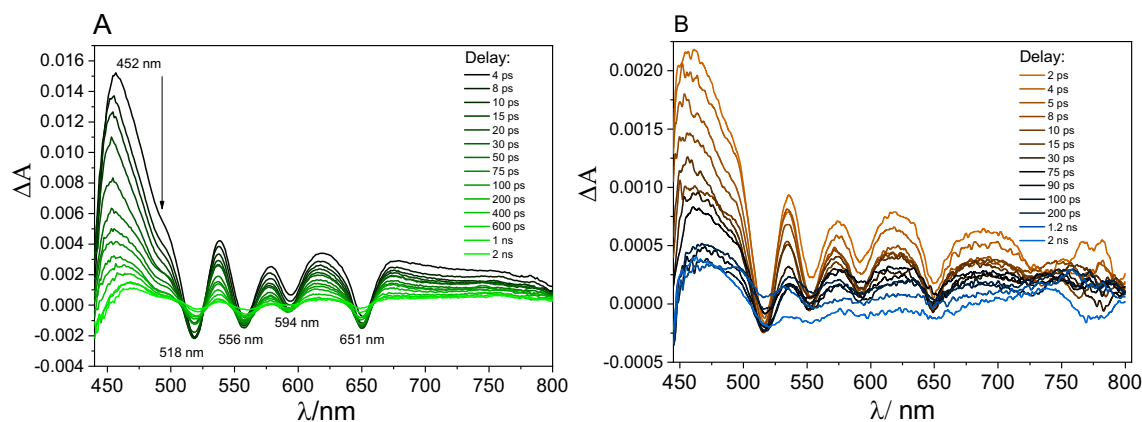


Figure 9. Transient absorption spectra registered at various time delays for: (A) TPPNH₂ and (B) GO-CONHTPP in DMF-H₂O (1:2, v/v) following the 422 nm laser excitation.

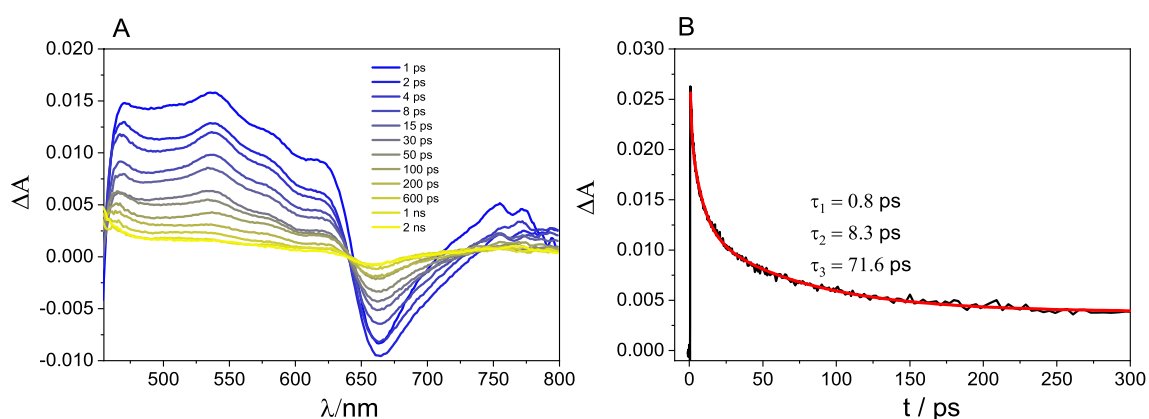


Figure 10. (A) Transient absorption spectra registered at various time delays and (B) absorption time profile probed at 550 nm measured for TPPNH₂ in the presence of GO (GO concentration 0.4 mg mL⁻¹) in DMF-H₂O (1:2, v/v) following the 440 nm laser excitation. Transient absorption spectra and kinetics are corrected for GO contribution.

time constants of 0.8 ps, 8.3 ps, and 71.6 ps, which can be explained by the fast back electron transfer (Fig. 10B). This is supported by the bleach recovery at 660 nm, which follows the same kinetics as the transient absorption decay at 550 nm. The three exponential decays of the TPPNH₂ radical cation signal presumably reflect various TPPNH₂ aggregates in GO nanoassemblies that may influence the rate constant of back electron transfer. Note the residual signal of about 15% in all kinetic profiles. This offset might be explained by the presence of TPPNH₂ radical cations, which did not undergo back electron transfer during the probed time window of 3 ns. The presence of long-lived charge-separated states indicates possible solar energy conversion systems applications.

Singlet oxygen generation. Evaluation of the ability of porphyrin/GO nano hybrids to produce reactive oxygen species can be valuable for predicting in vitro activity against cancer cells or microorganisms⁶⁰. Optically diluted solutions of free TPPNH₂, GO-CONHTPP, and the mixture of TPPNH₂ and GO in DMF were excited at 408 nm, and the photogeneration of singlet oxygen was measured by detecting its phosphorescence decay at $\lambda = 1270$ nm⁶¹. The singlet oxygen quantum yields ($\Phi\Delta$) in DMF were determined by comparison of the amplitudes of the decay curves collected for 10 min with that recorded for tris(2,2'-bipyridine)ruthenium(II) ($\Phi\Delta = 0.69$, DMF), used as a standard (Fig. 11)⁶². Tail fitting yielded a lifetime of 26 μ s, which agrees with published literature values for the lifetime of singlet oxygen in DMF⁶³.

The GO-CONHTPP was found to sensitize the production of singlet oxygen with a quantum efficiency ($\Phi\Delta = 0.20$) comparable to that of free TPPNH₂ ($\Phi\Delta = 0.26$). This supports the absence of GO interaction with the singlet excited state of porphyrin, which could suppress the efficient intersystem crossing and triplet state formation. In DMF-H₂O (1:2, v/v), the singlet oxygen decay amplitude was identical for free TPPNH₂ and GO-CONHTPP (Fig. S20). Noteworthy, TPPNH₂ attached non-covalently to GO in DMF is a photosensitizer with significantly lower singlet oxygen quantum yield ($\Phi\Delta = 0.08$) relative to free TPPNH₂. For the same non-covalent TPPNH₂/GO composite in DMF-H₂O (1:2, v/v) no singlet oxygen production was detected, confirming the involvement of electron transfer interactions between excited porphyrin and GO. Maintaining the singlet

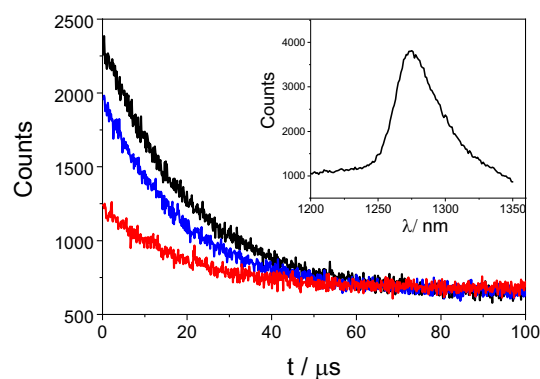


Figure 11. Decay curves of the singlet oxygen generated by free TPPNH₂ (black), GO-CONHTPP (blue) and a non-covalent mixture of TPPNH₂ and GO (red) in DMF ($\lambda_{\text{exc}} = 408 \text{ nm}$, $\lambda_{\text{mon}} = 1270 \text{ nm}$, collection time: 10 min). Inset: phosphorescence spectrum of ¹O₂ measured for TPPNH₂ in DMF.

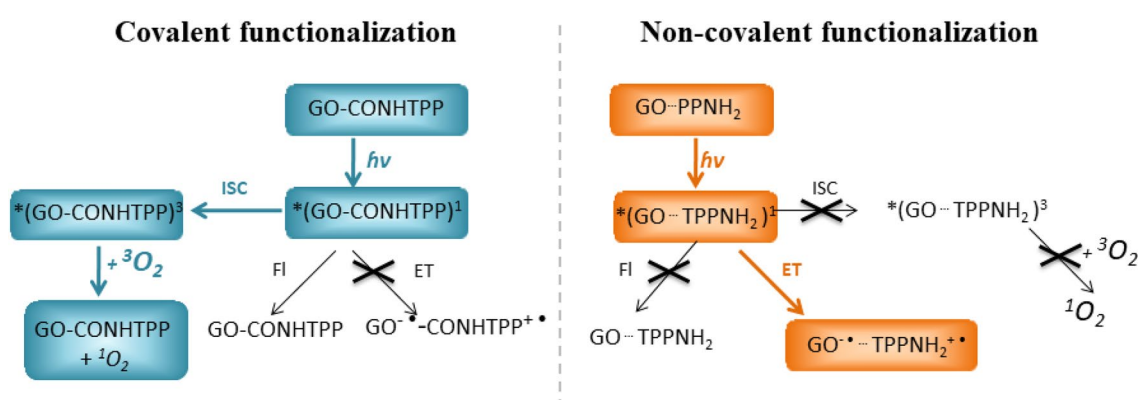


Figure 12. Possible deactivation paths of the excited states of GO-CONHTPP and GO-TPPNH₂ discussed in text (*FI* fluorescence, *ET* electron transfer). Deactivation paths important for practical application were marked in blue and orange for GO-CONHTPP and GO-TPPNH₂, respectively.

oxygen quantum efficiency by TPPNH₂ upon covalent functionalization to GO is an important outcome useful for designing graphene-based photosensitizers for photodynamic/photothermal therapy.

In summary, our spectroscopic experiments revealed significant differences between the deactivation pathways of the excited state of porphyrins depending on the type of functionalization with GO (Fig. 12). For GO-TPPNH₂ fast electron transfer from the singlet excited state of porphyrin to GO prevents the formation of the triplet excited state. As a result the ¹O₂ generation was suppressed. In contrary, for GO-CONHTPP the ¹O₂ generation yields was comparable to free TPPNH₂ what reflects weak interaction of the GO with the excited state of the porphyrins.

Quantum chemical calculations. We have recently validated a molecular model for graphene oxide that has been successfully used to gain insights into electronic structure changes upon non-covalent nanohybrids formation with various porphyrins^{25–27}. We note that carboxylic groups are placed at the GO system's terminal (equatorial) positions and can participate in the amide bond formation with a porphyrin. Such properties allow us to directly compare the electronic structure of the covalently and non-covalently bound hybrids studied in the present work. The free porphyrin has an expected structure and HOMO–LUMO gap (3.96 eV) similar to previously studied systems (Fig. 13)^{25–27}. The GO-CONHTPP hybrid features an amide bond in an expected *trans* configuration. Porphyrin and GO moieties are spatially well separated (distance between centers of mass of 17.0 Å) and oriented perpendicular to each other. The inspected dihedral angles of the porphyrin moiety are virtually indistinguishable from free TPPNH₂; this is reflected in almost unchanged energies of the corresponding molecular orbitals.

In contrast, the non-covalent hybrid displays stacking that favors the cofacial orientation of hybrid components. Consequently, the subsystems are close to each other (distance between centers of mass of 4.5 Å), and the TPPNH₂ molecule flattens as the C–C–C–C dihedral angles (green in Fig. 13), describing the out-of-plane rotation of the phenyl substituents decreases compared to free TPPNH₂. Such geometrical changes significantly impact the energies of the frontier molecular orbitals of the TPPNH₂ molecule. We observed a decrease in the energy difference between the corresponding orbital pairs compared to isolated porphyrin (e.g., from 3.96 to 3.82 eV), which explains the experimentally observed red-shift of the Soret band.

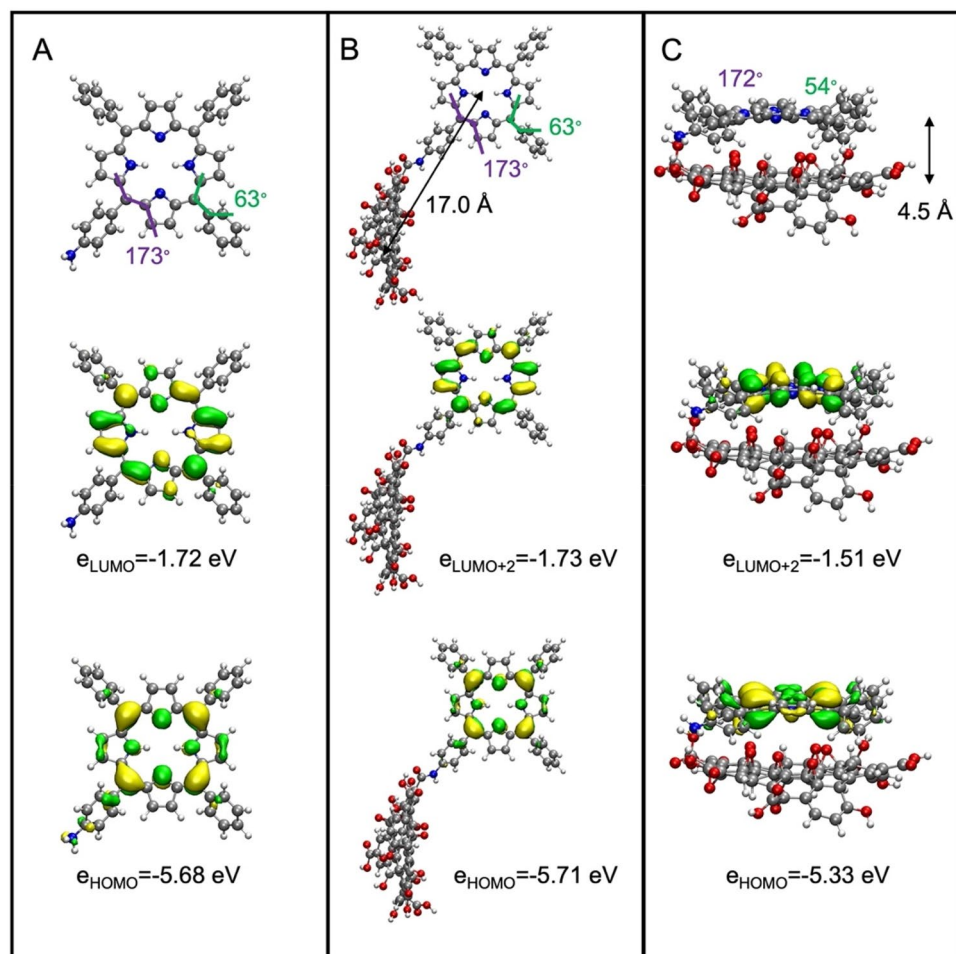


Figure 13. Calculated structures (BP86 + D3gCP/def2-TZVP; top) and selected frontier molecular orbitals strongly localized in the porphyrin moiety along with corresponding orbital energies (middle and bottom) for: (A) TPPNH₂, (B) GO-CONHTPP, and (C) GO/TPPNH₂ noncovalent hybrid. Molecular orbitals were computed at B3LYP/def2-TZVP level and drawn as ± 0.03 a.u. isosurfaces. Key dihedral angles are marked in color (purple and green), the distances between centers of mass between GO and porphyrin moieties are denoted by black arrows.

Consistent with our previous studies, the HOMO is strongly localized on porphyrin, while the first unoccupied MO is GO-centered. Thus, one might expect a low-energy charge-transfer excited state for porphyrin. However, we expect the probability of charge transfer to be very different between the two studied hybrids. We, therefore, computed an overlap integral $S_{H/L}$ between HOMO/LUMO pairs for covalently bound and non-covalently interacting hybrids to quantify this issue. This was negligibly small for the former ($S_{H/L} = 0.002$), while it was an order of magnitude more significant for the latter ($S_{H/L} = 0.069$). Thus, the probability of electron transfer, which is proportional to $S_{H/L}$, decreases when the porphyrin is covalently anchored to the GO.

Conclusions

Herein, it was demonstrated that while TPPNH₂ can be successfully assembled on the GO surface via either covalent or non-covalent bonding, the properties of these two types of hybrid materials differ significantly. The covalent attachment of TPPNH₂ was achieved through amide formation at the periphery of GO sheets and the hybrid material was fully characterized by FTIR, XPS, Raman spectroscopy, and SEM. Spectroscopic measurements together with theoretical calculations demonstrated that assembling TPPNH₂ on the GO surface in DMF-H₂O (1:2, v/v) via non-covalent interactions causes changes in the absorption spectra of porphyrin, as well as efficient quenching of its emission. Interestingly, covalent binding to GO does not affect notably neither the porphyrin absorption nor its fluorescence. Our results clearly demonstrate that the type of functionalization influences the perturbation of the ground state electronic structure of TPPNH₂ by GO. The structure of the covalent and non-covalent hybrid materials predicted by theoretical calculations indicates that close proximity and π - π -stacking of the porphyrin molecule with the GO sheet is possible only for the non-covalent functionalization. Therefore, it can be concluded that π - π -stacking interaction is required to modify the ground state electronic structure of porphyrin in the assembly. Secondly, femtosecond pump-probe experiments revealed

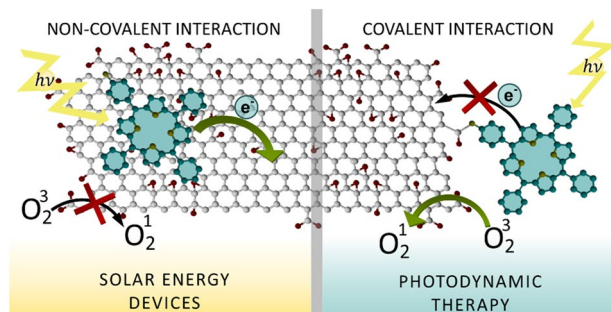


Figure 14. Schematic representation of the influence of the porphyrin/GO hybrid functionalization type on their interaction with light.

that only the non-covalent assembly of TPPNH₂ and GO enhances the efficiency of the photoinduced electron transfer from porphyrin to GO. Our results clearly demonstrate that although covalent functionalization prevents aggregation of the porphyrin molecules the electronic interaction of porphyrin and GO both in the ground and excited state, is limited. The negligible excited state interaction of porphyrin with GO in the covalent hybrid was reflected in its ability to generate singlet oxygen comparable to free TPPNH₂, thus indicating the feasibility of covalent hybrid materials for photodynamic/photothermal therapy (Fig. 14).

In summary, our results demonstrate that by covalently attaching TPPNH₂ to the GO, a material with sufficient yield of singlet oxygen generation is obtained, whereas non-covalent assembly leads to a material exhibiting efficient PET properties. This study provides valuable knowledge for developing highly efficient nanomaterials for desired applications.

Data availability

All data generated or analyzed during this study are included in this published article (and its Supplementary Information files).

Received: 13 April 2022; Accepted: 18 July 2022

Published online: 04 August 2022

References

- Ladomenou, K. *et al.* Photochemical hydrogen generation with porphyrin-based systems. *Coord. Chem. Rev.* **304**, 38–54. <https://doi.org/10.1016/j.ccr.2014.10.001> (2015).
- Zhang, Y., Ren, K., Wang, L., Wang, L. & Fan, Z. Porphyrin-based heterogeneous photocatalysts for solar energy conversion. *Chin. Chem. Lett.* **33**, 33–60. <https://doi.org/10.1016/j.ccl.2021.06.013> (2022).
- Min Park, J., Lee, J. H. & Jang, W.-D. Applications of porphyrins in emerging energy conversion technologies. *Coord. Chem. Rev.* **407**, 213157. <https://doi.org/10.1016/j.ccr.2019.213157> (2020).
- Ryan, A. A. & Senge, M. O. How green is green chemistry? Chlorophylls as a bioresource from biorefineries and their commercial potential in medicine and photovoltaics. *Photochem. Photobiol. Sci.* **14**, 638–660. <https://doi.org/10.1039/C4PP00435C> (2015).
- Kay, A. & Grätzel, M. Artificial photosynthesis. 1. Photosensitization of titania solar cells with chlorophyll derivatives and related natural porphyrins. *J. Phys. Chem.* **97**, 6272–6277. <https://doi.org/10.1021/j100125a029> (1993).
- Bonnett, R. Photosensitizers of the porphyrin and phthalocyanine series for photodynamic therapy. *Chem. Soc. Rev.* **24**, 19–33. <https://doi.org/10.1039/CS9952400019> (1995).
- Lovell, J. F., Liu, T. W. B., Chen, J. & Zheng, G. Activatable photosensitizers for imaging and therapy. *Chem. Rev.* **110**, 2839–2857. <https://doi.org/10.1021/cr900236h> (2010).
- Ethirajan, M., Chen, Y., Joshi, P. & Pandey, R. K. The role of porphyrin chemistry in tumor imaging and photodynamic therapy. *Chem. Soc. Rev.* **40**, 340–362. <https://doi.org/10.1039/B915149B> (2011).
- Wojcik, A. & Kamat, P. V. Reduced graphene oxide and porphyrin. An interactive affair in 2-d. *ACS Nano* **4**, 6697–6706. <https://doi.org/10.1021/nn102185q> (2010).
- Wang, Y. *et al.* A photoinduced electron transfer system by graphene oxide non-covalently linked porphyrin antennae in water. *Electrochemistry* **83**, 950–955. <https://doi.org/10.5796/electrochemistry.83.950> (2015).
- Larowska, D. *et al.* Graphene oxide functionalized with cationic porphyrins as materials for the photodegradation of rhodamine b. *J. Phys. Chem. C* **124**, 15769–15780. <https://doi.org/10.1021/acs.jpcc.0c03907> (2020).
- Aly, S. M., Parida, M. R., Alarousu, E. & Mohammed, O. F. Ultrafast electron injection at the cationic porphyrin–graphene interface assisted by molecular flattening. *Chem. Commun.* **50**, 10452–10455. <https://doi.org/10.1039/C4CC04985C> (2014).
- Zhu, M. *et al.* Surfactant assistance in improvement of photocatalytic hydrogen production with the porphyrin noncovalently functionalized graphene nanocomposite. *ACS Appl. Mater. Interfaces*. **5**, 1732–1740. <https://doi.org/10.1021/am302912v> (2013).
- Yuan, Y.-J. *et al.* Construction of a noble-metal-free photocatalytic H₂ evolution system using MoS₂/reduced graphene oxide catalyst and zinc porphyrin photosensitizer. *J. Phys. Chem. C* **121**, 24452–24462. <https://doi.org/10.1021/acs.jpcc.7b08290> (2017).
- Tian, B., Wang, C., Zhang, S., Feng, L. & Liu, Z. Photothermally enhanced photodynamic therapy delivered by nano-graphene oxide. *ACS Nano* **5**, 7000–7009. <https://doi.org/10.1021/nn201560b> (2011).
- Dias, L. D. & Mfouo-Tynga, I. S. Learning from nature: Bioinspired chlorin-based photosensitizers immobilized on carbon materials for combined photodynamic and photothermal therapy. *Biomimetics* **5**, 53 (2020).
- Huang, P. *et al.* Folic acid-conjugated graphene oxide loaded with photosensitizers for targeting photodynamic therapy. *Theranostics* **1**, 240–250. <https://doi.org/10.7150/thno.v01p0240> (2011).
- Liu, G., Qin, H., Amano, T., Murakami, T. & Komatsu, N. Direct fabrication of the graphene-based composite for cancer photo-therapy through graphite exfoliation with a photosensitizer. *ACS Appl. Mater. Interfaces* **7**, 23402–23406. <https://doi.org/10.1021/acsami.5b07432> (2015).

19. Georgakilas, V. *et al.* Functionalization of graphene: Covalent and non-covalent approaches, derivatives and applications. *Chem. Rev.* **112**, 6156–6214. <https://doi.org/10.1021/cr3000412> (2012).
20. Yu, W., Sisi, L., Haiyan, Y. & Jie, L. Progress in the functional modification of graphene/graphene oxide: A review. *RSC Adv.* **10**, 15328–15345. <https://doi.org/10.1039/D0RA01068E> (2020).
21. Monteiro, A. R., Neves, M. G. P. M. S. & Trindade, T. Functionalization of graphene oxide with porphyrins: Synthetic routes and biological applications. *ChemPlusChem* **85**, 1857–1880. <https://doi.org/10.1002/cplu.202000455> (2020).
22. Ladomenou, K. *et al.* Meso-substituted porphyrin derivatives via palladium-catalyzed amination showing wide range visible absorption: Synthesis and photophysical studies. *Inorg. Chem.* **51**, 10548–10556. <https://doi.org/10.1021/ic300714n> (2012).
23. Lewandowska-Andralojc, A. & Marciniak, B. Five major sins in fluorescence spectroscopy of light-harvesting hybrid materials. *ACS Energy Lett.* **4**, 1898–1901. <https://doi.org/10.1021/acscenergylett.9b01146> (2019).
24. Wendel, M. *et al.* Time-resolved spectroscopy of the singlet excited state of betanin in aqueous and alcoholic solutions. *Phys. Chem. Chem. Phys.* **17**, 18152–18158. <https://doi.org/10.1039/C5CP00684H> (2015).
25. Gacka, E., Burdzinski, G., Marciniak, B., Kubas, A. & Lewandowska-Andralojc, A. Interaction of light with a non-covalent zinc porphyrin–graphene oxide nanohybrid. *Phys. Chem. Chem. Phys.* **22**, 13456–13466. <https://doi.org/10.1039/D0CP02545C> (2020).
26. Gacka, E. *et al.* Noncovalent porphyrin–graphene oxide nanohybrids: The pH-dependent behavior. *J. Phys. Chem. C* **123**, 3368–3380. <https://doi.org/10.1021/acs.jpcc.8b11374> (2019).
27. Siklitskaya, A. *et al.* Lerf–Klinowski-type models of graphene oxide and reduced graphene oxide are robust in analyzing non-covalent functionalization with porphyrins. *Sci. Rep.* **11**, 7977. <https://doi.org/10.1038/s41598-021-86880-1> (2021).
28. Becke, A. D. Density-functional exchange-energy approximation with correct asymptotic behavior. *Phys. Rev. A* **38**, 3098–3100. <https://doi.org/10.1103/PhysRevA.38.3098> (1988).
29. Grimme, S., Antony, J., Ehrlich, S. & Krieg, H. A consistent and accurate ab initio parametrization of density functional dispersion correction (DFT-D) for the 94 elements H–PU. *J. Chem. Phys.* **132**, 154104. <https://doi.org/10.1063/1.3382344> (2010).
30. Grimme, S., Ehrlich, S. & Goerigk, L. Effect of the damping function in dispersion corrected density functional theory. *J. Comput. Chem.* **32**, 1456–1465. <https://doi.org/10.1002/jcc.21759> (2011).
31. Kruse, H. & Grimme, S. A geometrical correction for the inter- and intra-molecular basis set superposition error in Hartree–Fock and density functional theory calculations for large systems. *J. Chem. Phys.* **136**, 154101. <https://doi.org/10.1063/1.3700154> (2012).
32. Becke, A. D. A new mixing of Hartree–Fock and local density-functional theories. *J. Chem. Phys.* **98**, 1372–1377. <https://doi.org/10.1063/1.464304> (1993).
33. Weigend, F. & Ahlrichs, R. Balanced basis sets of split valence, triple zeta valence and quadruple zeta valence quality for H to Rn: Design and assessment of accuracy. *Phys. Chem. Chem. Phys.* **7**, 3297–3305. <https://doi.org/10.1039/B508541A> (2005).
34. Neese, F. Software update: The orca program system, version 4.0. *WIREs Comp. Mol. Sci.* **8**, e1327. <https://doi.org/10.1002/wcms.1327> (2018).
35. Lu, T. & Chen, F. Multiwfn: A multifunctional wavefunction analyzer. *J. Comput. Chem.* **33**, 580–592. <https://doi.org/10.1002/jcc.22885> (2012).
36. Albert, J. S. *et al.* *Encyclopedia of Reagents for Organic Synthesis*, Ch. 1–9 (Wiley, 2017).
37. König, W. & Geiger, R. Eine neue methode zur synthese von peptiden: Aktivierung der carboxylgruppe mit dicyclohexylcarbodiimid unter zusatz von 1-hydroxy-benzotriazolonen. *Chem. Ber.* **103**, 788–798. <https://doi.org/10.1002/cber.19701030319> (1970).
38. Krzyszkowska, E., Walkowiak-Kulikowska, J., Stienen, S. & Wojcik, A. Thionine–graphene oxide covalent hybrid and its interaction with light. *Phys. Chem. Chem. Phys.* **19**, 14412–14423. <https://doi.org/10.1039/C7CP01267E> (2017).
39. Łowicki, D. *et al.* Structural and antimicrobial studies of a new n-phenylamide of monensin a complex with sodium chloride. *J. Mol. Struct.* **923**, 53. <https://doi.org/10.1016/j.molstruc.2009.01.056> (2009).
40. Rachwal, S. & Katritzky, A. R. In *Comprehensive Heterocyclic Chemistry II: A Review of the Literature 1982–1995* (eds Katritzky, A. *et al.*) 1–158 (Elsevier, 2008).
41. Karousis, N. *et al.* Graphene oxide with covalently linked porphyrin antennae: Synthesis, characterization and photophysical properties. *J. Mater. Chem.* **21**, 109–117. <https://doi.org/10.1039/C0JM00991A> (2011).
42. Macquet, J. P., Millard, M. M. & Theophanides, T. X-ray photoelectron spectroscopy of porphyrins. *J. Am. Chem. Soc.* **100**, 4741–4746. <https://doi.org/10.1021/ja00483a018> (1978).
43. Papageorgiou, A. C. *et al.* Self-terminating protocol for an interfacial complexation reaction in vacuo by metal–organic chemical vapor deposition. *ACS Nano* **7**, 4520–4526. <https://doi.org/10.1021/nn401171z> (2013).
44. Xu, Y. *et al.* A graphene hybrid material covalently functionalized with porphyrin: Synthesis and optical limiting property. *Adv. Mater.* **21**, 1275–1279. <https://doi.org/10.1002/adma.200801617> (2009).
45. Zare-Dorabei, R., Rahimi, R., Koochi, A. & Zargari, S. Preparation and characterization of a novel tetrakis(4-hydroxyphenyl) porphyrin–graphene oxide nanocomposite and application in an optical sensor and determination of mercury ions. *RSC Adv.* **5**, 93310–93317. <https://doi.org/10.1039/C5RA17047H> (2015).
46. Zhang, X., Hou, L., Richard, F. & Samori, P. Modular preparation of graphene-based functional architectures through two-step organic reactions: Towards high-performance energy storage. *Chem. Eur. J.* **24**, 18518–18528. <https://doi.org/10.1002/chem.201803184> (2018).
47. Ahmed, A. *et al.* Covalently linked porphyrin–graphene oxide nanocomposite: Synthesis, characterization and catalytic activity. *J. Mater. Sci. Mater. Electron.* **30**, 19738–19751. <https://doi.org/10.1007/s10854-019-02324-7> (2019).
48. Neta, P. & Harriman, A. Zinc porphyrin π -radical cations in aqueous solution. Formation, spectra and decay kinetics. *J. Chem. Soc. Faraday Trans. 2* (81), 123–138. <https://doi.org/10.1039/F29858100123> (1985).
49. Neta, P., Richoux, M.-C., Harriman, A. & Milgrom, L. R. Resonance stabilisation of zinc porphyrin π -radical cations. *J. Chem. Soc. Faraday Trans. 2* (82), 209–217. <https://doi.org/10.1039/F29868200209> (1986).
50. Kano, K., Fukuda, K., Wakami, H., Nishiyabu, R. & Pasternack, R. F. Factors influencing self-aggregation tendencies of cationic porphyrins in aqueous solution. *J. Am. Chem. Soc.* **122**, 7494–7502. <https://doi.org/10.1021/ja000738g> (2000).
51. Kano, K., Minamizono, H., Kitae, T. & Negi, S. Self-aggregation of cationic porphyrins in water. Can π – π stacking interaction overcome electrostatic repulsive force? *J. Phys. Chem. A* **101**, 6118–6124. <https://doi.org/10.1021/jp9710446> (1997).
52. Kubát, P., Lang, K., Procházková, K. & Anzenbacher, P. Self-aggregates of cationic meso-tetratolylporphyrins in aqueous solutions. *Langmuir* **19**, 422–428. <https://doi.org/10.1021/la026183f> (2003).
53. Liu, Q.-Y. *et al.* Original article. *Chin. Chem. Lett.* **25**, 752–756. <https://doi.org/10.1016/j.ccl.2013.12.023> (2014).
54. Micali, N., Mallamace, F., Romeo, A., Purrello, R. & Monsù Scolaro, L. Mesoscopic structure of meso-tetrakis(4-sulfonatophenyl) porphine j-aggregates. *J. Phys. Chem. B* **104**, 5897–5904. <https://doi.org/10.1021/jp991909a> (2000).
55. Weinkauff, J. R., Cooper, S. W., Schweiger, A. & Wamser, C. C. Substituent and solvent effects on the hyperporphyrin spectra of diprotonated tetraphenylporphyrins. *J. Phys. Chem. A* **107**, 3486–3496. <https://doi.org/10.1021/jp022046f> (2003).
56. Senge, M. O. A conformational study of 5,10,15,20-tetraalkyl-22H⁺,24H⁺-porphyrindium salts (dication salts). *Zeitschrift für Naturforschung B* **55**, 336–344. <https://doi.org/10.1515/znb-2000-3-417> (2000).
57. White, W. I. In *The Porphyrins* Vol. 5 (ed. Dolphin, D.) 303 (Academic Press, 1978).
58. Wen, X. *et al.* Ultrafast electron transfer in the nanocomposite of the graphene oxide–Au nanocluster with graphene oxide as a donor. *J. Mater. Chem. C* **2**, 3826–3834. <https://doi.org/10.1039/C3TC32376E> (2014).
59. Masih, D., Aly, S. M., Usman, A., Alarousi, E. & Mohammed, O. F. Real-time observation of ultrafast electron injection at graphene–Zn porphyrin interfaces. *Phys. Chem. Chem. Phys.* **17**, 9015–9019. <https://doi.org/10.1039/C4CP06050D> (2015).

60. Callaghan, S. & Senge, M. O. The good, the bad, and the ugly—Controlling singlet oxygen through design of photosensitizers and delivery systems for photodynamic therapy. *Photochem. Photobiol. Sci.* **17**, 1490–1514. <https://doi.org/10.1039/C8PP00008E> (2018).
61. Jiménez-Banzo, A., Ragàs, X., Kapusta, P. & Nonell, S. Time-resolved methods in biophysics. 7. Photon counting vs. analog time-resolved singlet oxygen phosphorescence detection. *Photochem. Photobiol. Sci.* **7**, 1003–1010. <https://doi.org/10.1039/B804333G> (2008).
62. Spiller, W. *et al.* Singlet oxygen quantum yields of different photosensitizers in polar solvents and micellar solutions. *J. Porphy. Phthalocyanines* **02**, 145–158. [https://doi.org/10.1002/\(sici\)1099-1409\(199803/04\)2:2%3c145::aid-jpp60%3e3.0.co;2-2](https://doi.org/10.1002/(sici)1099-1409(199803/04)2:2%3c145::aid-jpp60%3e3.0.co;2-2) (1998).
63. Oelckers, S., Hanke, T. & Röder, B. Quenching of singlet oxygen in dimethylformamide. *J. Photochem. Photobiol. A* **132**, 29–32. [https://doi.org/10.1016/S1010-6030\(99\)00247-6](https://doi.org/10.1016/S1010-6030(99)00247-6) (2000).

Acknowledgements

ALA acknowledges support by the National Science Centre grant no. 2015/19/D/ST5/00682. AK acknowledges support from the National Science Centre, Poland, grant number 2018/30/E/ST4/00004. Access to high performance computing resources was provided by the Interdisciplinary Centre for Mathematical and Computational Modelling in Warsaw, Poland, under grant GB79-5. M.O.S. was supported by the Technical University of Munich—Institute for Advanced Study through a Hans Fischer Senior Fellowship and acknowledges funding from Science Foundation Ireland (IvP 13/IA/1894).

Author contributions

A.L.-A.: conceptualization, investigation, methodology, and writing—original draft, supervision, E.G.: investigation, T.P.: methodology, G.B.: methodology, A.L.: investigation, J.M.O.: investigation, M.O.S.: writing—review and editing, A.S.: investigation, A.K.: investigation, methodology, B.M.: writing: review and editing, J.W.-K.: conceptualization, investigation and writing: review and editing.

Competing interests

The authors declare no competing interests.

Additional information

Supplementary Information The online version contains supplementary material available at <https://doi.org/10.1038/s41598-022-16931-8>.

Correspondence and requests for materials should be addressed to A.L.-A.

Reprints and permissions information is available at www.nature.com/reprints.

Publisher's note Springer Nature remains neutral with regard to jurisdictional claims in published maps and institutional affiliations.



Open Access This article is licensed under a Creative Commons Attribution 4.0 International License, which permits use, sharing, adaptation, distribution and reproduction in any medium or format, as long as you give appropriate credit to the original author(s) and the source, provide a link to the Creative Commons licence, and indicate if changes were made. The images or other third party material in this article are included in the article's Creative Commons licence, unless indicated otherwise in a credit line to the material. If material is not included in the article's Creative Commons licence and your intended use is not permitted by statutory regulation or exceeds the permitted use, you will need to obtain permission directly from the copyright holder. To view a copy of this licence, visit <http://creativecommons.org/licenses/by/4.0/>.

© The Author(s) 2022